Characterizing Interfacial Sliding of Through-Silicon-Via by Nano-Indentation

Chenglin Wu, Rui Huang, and Kenneth M. Liechti

***Abstract*—In this paper, an experimental method is proposed to determine the shear sliding behavior of the interface between a copper through-silicon-via (TSV) and silicon. This interface was loaded in a nano-indentation experiment on specimens that were fabricated using focused-ion-beam milling. The elastic and plastic properties of the copper via were first characterized by micro-pillar compression experiments. The interfacial sliding is described by a cohesive zone model with a traction-separation relation including a linearly elastic part followed by frictional sliding at a constant shear traction. Both analytical and numerical models were developed for extracting the parameters of the traction-separation relation for the shear behavior of the interface. The average critical shear traction required to initiate interfacial sliding was found to be 77.2 MPa and the corresponding relative displacement across the interface was 182.7 nm, while the frictional shear strength was 25 MPa. The traction-separation relation with the extracted parameters may be used to study via extrusion and associated reliability analysis for integrated TSV structures.**

***Index Terms*—Through-silicon via, interfacial sliding, nano-indentation, traction-separation relation.**

I. Introduction

In 3D integrated circuits (ICs), the through-silicon via (TSV) is a critical element connecting die-to-die in the integrated stack structure [1]. The interface between TSV and silicon plays an important role in determining the reliability and performance of the 3D ICs [2]. In particular, via extrusion has been identified as a major concern for the yield and reliability of 3D integration [3]–[6]. Previous studies based on modeling have suggested that via extrusion may be suppressed by improving the interfacial adhesion between TSV and silicon to resist sliding [7]. However, experimental characterization of the interfacial properties of TSV has been challenging. In this paper, we propose an experimental method to characterize the shear sliding behavior of the interface between a copper TSV and silicon by nano-indentation.

Manuscript received September 5, 2016; revised December 23, 2016 and February 3, 2017; accepted March 9, 2017. Date of publication March 13, 2017; date of current version June 5, 2017. This work was supported by the Semiconductor Research Corporation.

C. Wu is with Materials Research Center and Department of Civil, Architectural, and Environmental Engineering, Missouri University of Science and Technology, Rolla, MO 65409 USA (e-mail: wuch@mst.edu).

R. Huang and K. M. Liechti are with the Department of Aerospace Engineering and Engineering Mechanics, University of Texas, Austin, TX 78712 USA (e-mail: ruihuang@mail.utexas.edu).

Color versions of one or more of the figures in this paper are available online at http://ieeexplore.ieee.org.

Digital Object Identifier 10.1109/TDMR.2017.2681580

The nano-indentation experiment used in this study may be considered a variation of the fiber pushout test that is commonly used to characterize fiber/matrix interfaces in composite materials [8]. Because of the micro-scale dimensions of TSVs, nano-indentation experiments are ideal to characterize their properties and interactions with the silicon matrix. While such experiments have yet to be used for this purpose, similar experiments have been used to examine the compressive behavior of micro pillars. Typically, the micro-scale specimens are prepared through focused ion beam (FIB) milling [9], which is suitable for both copper and silicon specimens [10]. In this work, FIB was used to prepare copper micro pillars and pushout specimens from the same TSV structure, with which the elastic-plastic behavior of the copper TSV and the interfacial properties were characterized. In addition, a cohesive zone model was used to describe the interfacial sliding of TSVs with a traction-separation relation. An analytical shear-lag model and more detailed finite element analyses were used to guide the extraction of the traction-separation relation from the nano-indentation experiment. The resulting relation can then be used for the reliability analysis of integrated TSV structures.

II. Experiments

Two different experiments were conducted: (1) copper micro-pillar compression experiment; (2) copper via pushout experiment. The micro-pillar experiment was used to determine the elastic and plastic properties of the copper via, while the pushout experiment revealed the interfacial sliding behavior between the via and its silicon matrix. Both experiments were conducted using a nano-indenter (Agilent XP) with a truncated cone probe as the loading device. The specimens were prepared from an integrated TSV structure using a FIB/SEM dual beam system, which contains both ion beam and electron beam columns, intersecting at an angle of 52°. This allowed the specimens to be milled with accurate control of depth.

A. Micro-Pillar Compression Experiment

The as-received TSV structure contained periodic arrays of blind Cu vias in a 780 μm (001) Si wafer (Fig. 1). The nominal via diameter and depth were 10 and 55 μm, respectively. The spacing between the copper vias was 40 μm along the (100) direction and 50 μm along the (110) direction of the silicon wafer. To prepare the micro-pillar specimen, the silicon wafer was diced and polished until one row of the vias was about

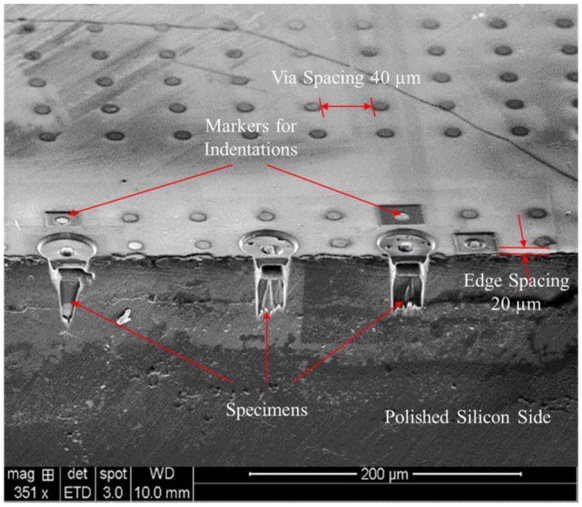

Fig. 1. Bird's eye view of the TSV structure with three pushout specimens prepared using FIB at the edge.

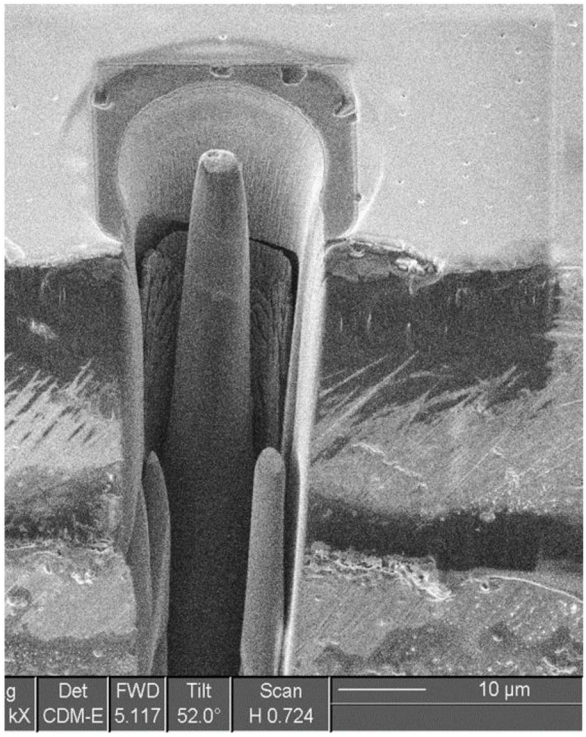

Fig. 2. Copper micro-pillar specimen prepared by FIB.

20 μm away from the polished side. For each micro-pillar specimen, the top 100 nm was milled off in order to eliminate the effect of surface roughness. Then the silicon surrounding the selected via was milled down by 3 μm in a concentric ring. The inner radius was the same as the via diameter (10 μm). The outer radius was 18 μm. Subsequently, a second ring pattern with a smaller outer radius (13 μm) was used to mill off the silicon immediately surrounding the copper pillar to a nominal depth of 55 μm. Finally, additional silicon was removed to expose the side of the micro-pillar (Fig. 2). Due to the ion beam divergence, the obtained copper micro-pillar was tapered by an angle of 2° with a 6-μm diameter at the top.

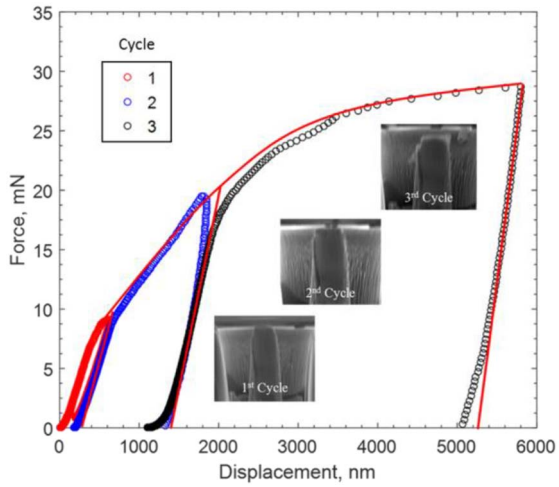

Fig. 3. The force-displacement response of a copper micro-pillar specimen over three loading/unloading cycles, comparing experimental data with FEA results (solid line).

The micro-pillar compression experiment was conducted using the nano-indenter with a truncated cone probe with an 8 μm tip diameter at a rate of 1 nm/s. A total of three loading/unloading cycles were applied with prescribed maximum displacements of 500, 1800, and 6000 nm. The force-displacement responses are shown in Fig. 3. For comparison, a finite element analysis was conducted to simulate the elastic-plastic deformation of the copper micro-pillar, adopting the associated flow model with isotropic hardening [11]. The Ramberg-Osgood equation was used to describe the relationship between the plastic strain and stress:

$$\varepsilon_p = \frac{3}{7}\frac{\sigma_e}{E}\left(\frac{\sigma_e}{\sigma_0}\right)^{n-1} \tag{1}$$

where ε_p is the equivalent plastic strain, σ_e is the equivalent stress, σ_0 is the yield stress, E is Young's modulus, and n is the hardening exponent. The Ramberg-Osgood equation [12] is commonly used to describe the nonlinear relationship between stress and strain (the stress-strain diagram), especially for metals with a smooth elastic-plastic transition and strain hardening. For the copper via, we set E to be 110 GPa and determined σ_0 and n based on the load-displacement response from the micro-pillar compression experiment. By taking the yield stress to be 216 MPa and the hardening exponent to be 3, the finite element analysis yielded a force-displacement response which is in close agreement with the experimental data (Fig. 3). The value of yield strength is similar to those obtained from previous measurements on copper TSVs [6], [13]. The corresponding von Mises stress and equivalent plastic strains are shown in Fig. 4a, with contour plots showing a slight gradient due to the tapered cross-section of the micro-pillar specimen. For the same nominal yield strength, higher hardening exponents lead to softer force-displacement responses (Fig. 4b). The obtained strain hardening exponent ($n = 3$) is smaller than the typical value of 5 for bulk copper [14], indicating that the copper TSVs have a stronger hardening response, possibly due to relatively small grain sizes [6].

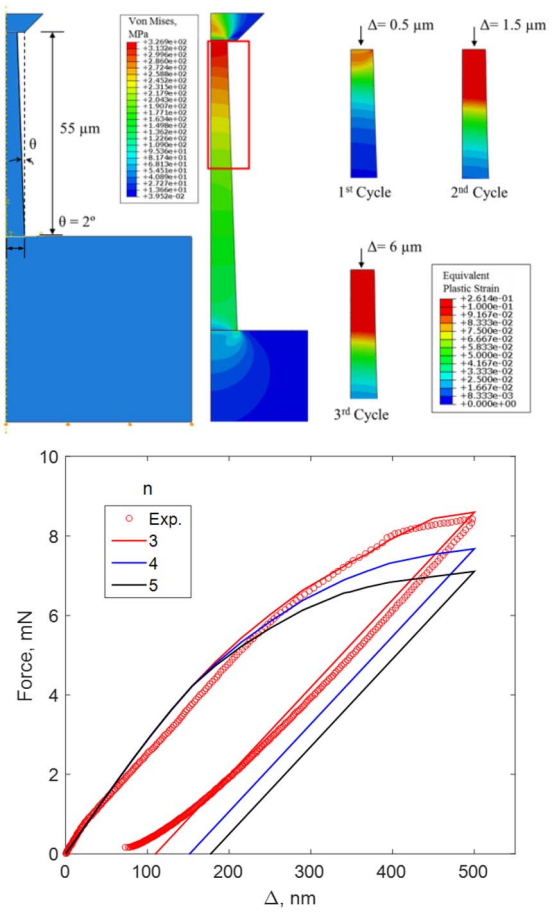

Fig. 4. Finite element model of micro-pillar compression: (a) stress and plastic strain contours; (b) effect of hardening exponent on force-displacement response.

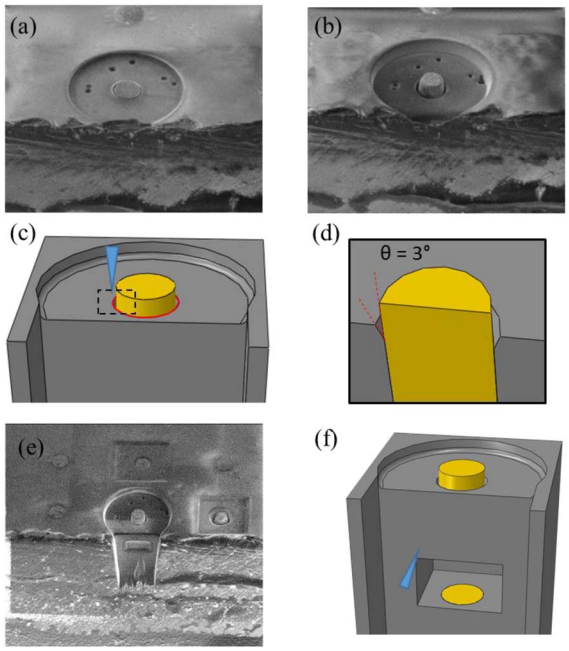

Fig. 5. FIB milling of a via pushout specimen: (a) top surface removal; (b) forming an annular crack; (c) forming a draft angle of 3°; (d) free-standing via with an annular crack; (e) a schematic of side opening and (f) edge view of side opening in process.

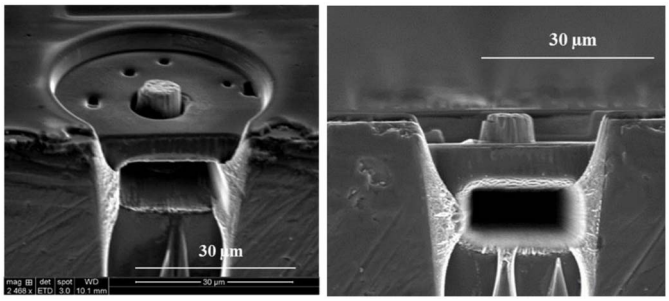

Fig. 6. The via pushout specimen: (a) 52 degree tilted view; (b) side view.

B. Via Pushout Experiment

The specimen preparation for the via pushout experiments (Fig. 5) was similar to the preparation of the micro-pillar specimens. About 100 nm of surface material was first removed to obtain a smooth top surface (Fig. 5a). The ring pattern milling was then performed to obtain a 3 μm free-standing portion of the via (Fig. 5b). An annular wedge crack with a draft angle of 3° was introduced by controlling the beam energy to 30 kPa with a working distance of 7 mm (Fig. 5c). The resulting annular crack was about 1μm as shown in Fig. 5d. After this, the blind via was turned into a through via (Fig. 5 e-f) by milling away the silicon and copper from the side at a distance of 6 μm below the front of the annular crack. The final specimen is shown in Fig. 6, which has a total via length of 9 μm and a bonded length of 5 μm.

The pushout experiment was performed with the truncated cone tip under a prescribed displacement loading protocol of 1 nm/s. The force-displacement responses for three specimens are shown in Fig. 7. When the force was lower than 6 mN, there was a linearly elastic relationship between the force and displacement. This indicates that the copper via remained elastic and no crack growth had occurred. Once the force level exceeded 6 mN, a slightly nonlinear response can be observed, which could be the result of either copper plasticity or crack growth or both. Remarkably, the force reached a peak value of approximately 12 mN, followed by a sudden drop under the displacement-controlled loading, which was most likely due to unstable crack growth along the interface. Subsequently, the indentation force remained constant (∼4 mN) as the indenter continued pushing the via, which suggests frictional sliding between the via and the surrounding silicon. Unloading at this stage showed elastic characteristics with the same slope as the initial elastic response. Based on the average measured peak force (∼12 mN), the interfacial shear strength was initially estimated to be 76 MPa, assuming a contact area based on the bonded length and the via diameter. The constant sliding force provided an estimate of the steady-state frictional shear strength of about 25 MPa.

Moreover, SEM images of the specimen (Fig. 8a) after the pushout experiment show clear evidence of interfacial sliding but no severe plastic deformation at the top of the via. This suggests that plastic deformation of the copper via was limited due to relatively low indentation forces. On the other hand, with an initial crack at the interface and a relatively small

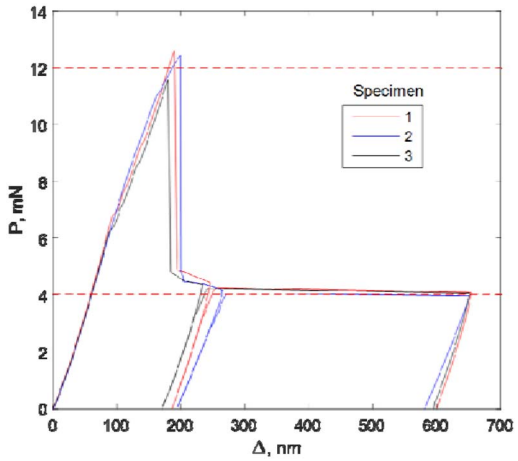

Fig. 7. The force-displacement responses of via pushout experiments.

TABLE I
ELEMENT COMPOSITION FROM EDS OF THE INTERFACE AFTER PUSHOUT

Element	Weight (%)	Sigma (%)
Cu	74.34	0.08
Si	10.82	0.03
Ta	1.09	0.08
Fe	0.04	0.01
Os	0.01	0.0018

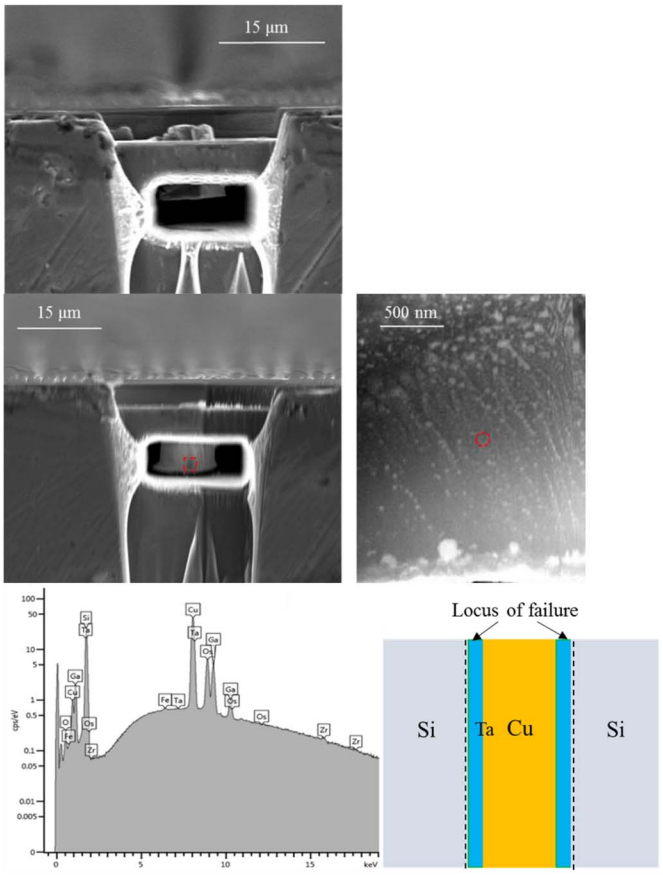

Fig. 8. Identification of the locus of failure: (a) post-failure view of a via pushout specimen; (b) exposed surface of a via that has been pushed out; (c) EDS of a via fracture surface; (d) schematic of the failure locus.

interfacial area, the force was sufficient to cause unstable crack growth along the interface and subsequent frictional sliding.

The interface was further examined using energy-dispersive X-ray spectroscopy (EDS) after pushing the via out to expose the via side of the interface through the etching window (Fig. 8b). The red dashed square identifies the region (Fig. 8b) where the spot for the EDS spectrum (Fig. 8c) was located. The beam energy for the EDS was set at 30 keV, which allowed a depth of 1.5 to 2 μm of the exposed surface to be probed. Given that the tantalum layer is 5-10 nm thick, this energy level is sufficient to probe any silicon remaining on the via as well as the copper and the tantalum. The obtained composition data are listed in Table I, where it can be seen that the strongest signal was from copper (74.3%), followed by silicon (10.8%) and tantalum (1.1%). Tantalum is commonly used as a barrier layer between the copper via and the silicon matrix. The presence of silicon on the via side of the interface suggests that the crack growth and sliding occurred close to the interface between silicon and the tantalum barrier layer as illustrated schematically in Fig. 8d. Note that the EDS signals are based on back scattered electrons from the copper which pass through the tantalum and silicon on their way to the sensor.

III. ANALYSIS AND RESULTS

The stress and fracture analyses associated with the via pushout experiment were conducted at three levels. The first was a shear lag analysis, which was motivated by the measured load-displacement response. This was followed by finite element analyses, first based on linearly elastic fracture mechanics and then a specialized cohesive zone model, both using the commercial finite element code ABAQUS®.

A. Shear Lag Analysis

Previously, a shear lag model was developed to predict initiation and growth of interfacial delamination in TSV structures [15]. The model essentially combined force balance in the axial direction of the via with a shear traction at the interface through a traction-separation relation. In developing a shear lag analysis for the TSV pushout experiment (Fig. 9a), it was assumed that the indenter was a rigid flat punch that imposed a uniform normal traction and end displacement (Δ) to the top of the via (excluding the extruded part). The copper via was assumed to be linearly elastic in a rigid silicon matrix. For each differential element of the via (Fig. 9b), the difference of the axial stresses (σ_f) on the two cross-sections is balanced by the shear traction (τ) on the side face due to via-silicon interactions at the interface. The force balance of the differential element requires that

$$\tau = -\frac{D_f}{4}\frac{d\sigma_f}{dx} \tag{2}$$

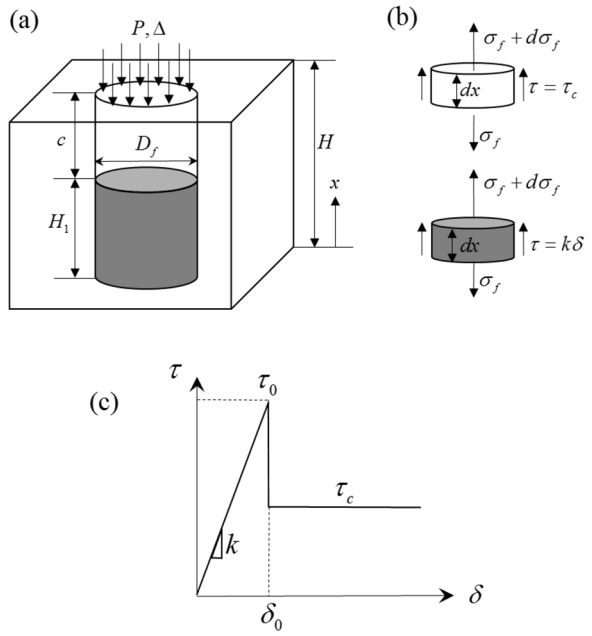

Fig. 9. A shear lag model: (a) schematic of the via pushout experiment; (b) free body diagrams; (c) a shear traction-separation relation for the interface.

where D_f is the via diameter. The axial stress in the via is related to its axial displacement (u_f) through Hooke's law of linear elasticity:

$$\sigma_f = E_f \frac{du_f}{dx} \tag{3}$$

where E_f is Young's modulus of copper.

The relative displacement across the interface is: $\delta = u_m - u_f$, where $u_m \approx 0$ by the assumption of a rigid silicon matrix. The shear traction and the relative displacement are related by a shear traction-separation relation. Motivated by the measured load-displacement response, the interface between the via and silicon was assumed to follow a shear traction-separation relation with two segments (Fig. 9c), first linearly elastic (before fracture) and then a constant traction for frictional sliding, i.e.,

$$\tau = \begin{cases} k\delta, & \delta \le \delta_0 \\ \tau_c, & \delta_0 < \delta \end{cases} \tag{4}$$

where k is the initial stiffness of the interface, δ_0 is the critical displacement for fracture, and τ_c is the frictional shear strength of the interface. Correspondingly, the peak traction is $\tau_0 = k\delta_0$.

When the end displacement $\Delta < \delta_0$, the relative displacement δ is less than δ_0 everywhere and thus the traction-separation relation is linearly elastic ($\tau = k\delta$). In this case, substituting Eqs. (3) and $(4)_1$ into Eq. (2) results in (with $\delta = -u_f$)

$$\frac{E_f D_f}{4k}\frac{d^2\delta}{dx^2} = \delta \tag{5}$$

Solving Eq. (5) with proper boundary conditions, we obtain that

$$\delta = \Delta \frac{\cosh\left(\frac{x}{\lambda}\right)}{\cosh\left(\frac{H}{\lambda}\right)} \tag{6}$$

where $\lambda = \sqrt{\frac{E_f D_f}{4k}}$ is a characteristic length and H is the initial bonded length of the specimen. Here we have used two boundary conditions: end displacement on top ($\delta = \Delta$ at $x = H$) and zero axial force at bottom ($\sigma_f = 0$ at $x = 0$). The corresponding axial stress in the via is then obtained by inserting (6) into (3), and the resultant indentation force is

$$P = \frac{\pi D_f^2 E_f \Delta}{4\lambda} \tanh\left(\frac{H}{\lambda}\right) \tag{7}$$

which gives a linear force-displacement relation as the first stage of the pushout experiment.

When the applied end displacement $\Delta > \delta_0$, part of the interface undergoes frictional sliding with $\delta > \delta_0$ while the other part remains linearly elastic with $\delta < \delta_0$. Let H_1 be the length of the via where the interface remains linearly elastic (Fig. 9a). For this part ($0 < x < H_1$), we solve Eq. (5) with $\delta = \delta_0$ at $x = H_1$ as a boundary condition to obtain

$$\delta = \delta_0 \frac{\cosh\left(\frac{x}{\lambda}\right)}{\cosh\left(\frac{H_1}{\lambda}\right)} \tag{8}$$

For the upper part ($H_1 < x < H$), the constant shear traction in Eq. $(4)_2$ is substituted into Eq. (2), which leads to

$$\frac{E_f D_f}{4}\frac{d^2\delta}{dx^2} = \tau_c, \tag{9}$$

Integrating Eq. (9) we obtain

$$\delta = \frac{2\tau_c}{E_f D_f}x^2 + C_1 x + C_2, \tag{10}$$

where C_1 and C_2 are coefficients to be determined from the boundary conditions. Applying the displacement and stress continuity conditions at $x = H_1$, we obtain

$$C_1 = \frac{\delta_0}{\lambda}\tanh\left(\frac{H_1}{\lambda}\right) - \frac{4\tau_c H_1}{E_f D_f}$$
$$C_2 = \delta_0\left[1 - \frac{H_1}{\lambda}\tanh\left(\frac{H_1}{\lambda}\right)\right] + \frac{2\tau_c H_1^2}{E_f D_f} \tag{11}$$

Furthermore, applying the end displacement condition at $x = H$, we obtain an equation for determining H_1 or equivalently, the sliding zone size $c = H - H_1$:

$$f = \frac{\Delta}{\delta_0} - 1 - \tanh\left(\frac{H-c}{\lambda}\right)\frac{c}{\lambda} - \frac{2\tau_c}{E_f D_f \delta_0}c^2 = 0. \tag{12}$$

Acceptable values of c (i.e., $0 < c < H$) are obtained from Eq. (12) when $\Delta > \delta_0$ and $\Delta < \Delta_c$, where

$$\Delta_c = \delta_0 + \frac{2\tau_c}{E_f D_f}H^2. \tag{13}$$

Correspondingly, the indentation force is obtained as

$$P = \frac{\pi D_f^2}{4}\left[\frac{4\tau_c c}{D_f} + \frac{E_f \delta_0}{\lambda}\tanh\left(\frac{H-c}{\lambda}\right)\right]. \tag{14}$$

When $\Delta \ge \Delta_c$, the entire interface undergoes frictional sliding ($c = H$). In this case, we have

$$P = \pi D_f \tau_c H, \tag{15}$$

which is a constant, independent of Δ.

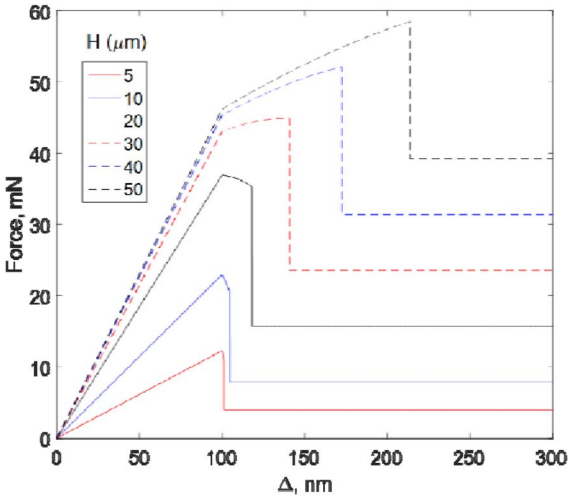

Fig. 10. Force-displacement responses of the via pushout experiment predicted by the shear-lag analysis showing the effect of the bonded length.

The force-displacement response of the push-out experiment predicted by the shear lag model consists of three segments: a linearly elastic segment (Eq. 7), an intermediate nonlinear segment (Eq. 14), and a constant force segment (Eq. 15). It is found that the force-displacement response depends sensitively on the bonded length (H) of the specimen (Fig. 10). In this case, we take $\delta_0 = 100$ nm, $k = 0.8$ MPa/nm and $\tau_c = 25$ MPa for the purpose of discussion. With the same traction-separation relation, a larger bonded length results in a stiffer initial load-displacement response and hence higher loads in all three segments. The response in the second segment is of particular interest, where the interface is partially elastic and partially frictional. For a relatively long specimen (H $> 20\mu$m), the force increases as the indenter displacement increases, but the slope is lower than the elastic segment. For a shorter specimen (H $< 20\mu$m), the force decreases with increasing displacement. In all cases, the force drops abruptly at $\Delta = \Delta_c$, after which the interface is fully frictional and the force remains constant. The discontinuous drop of the indentation force is a result of the assumed discontinuous traction-separation relation for the interface. By Eq. (12), there are two possible solutions for the sliding zone size c. Prior to the drop ($\Delta < \Delta_c$), one solution is greater than the bonded length and thus eliminated. When $\Delta = \Delta_c$, both solutions are acceptable and one of them corresponds to the fully sliding case with $c = H$. As a result, the associated indentation force drops abruptly from the partially sliding solution to the fully sliding solution.

Interestingly, the shear-lag analysis predicts that the intermediate segment between the linearly elastic ($\Delta < \delta_0$) and fully frictional ($\Delta \geq \Delta_c$) segments of the force-displacement response diminishes as the specimen length decreases. For H $= 5\mu$m, the force-displacement response appears to have only two segments as the intermediate segment becomes negligibly small. In this case, $\frac{\Delta_c - \delta_0}{\delta_0} = \frac{2\tau_c}{E_f D_f \delta_0} H^2 << 1$, and the force-displacement response from the indentation experiment can be directly converted to the traction-separation relation of the interface. Specifically,

TABLE II
EXTRACTED PARAMETERS FOR THE TRACTION-SEPARATION RELATION

	Specimen	k (MPa/nm)	δ_0 (nm)	τ_0 (MPa)	τ_c (MPa)	J_{II} (J/m^2)
Analytical	1	0.418	189.0	79.0	25	7.47
	2	0.392	199.3	78.2	25	7.79
	3	0.402	179.8	72.2	25	6.49
Numerical	1	0.450	179.0	80.5	25	7.20
	2	0.407	193.6	78.8	25	7.63
	3	0.412	175.5	72.4	25	6.35

the slope of the linearly elastic response can be used to determine the stiffness k via Eq. (7), the displacement at the peak force gives the critical separation δ_0, and the constant force in the fully frictional segment can be converted to the frictional shear strength τ_c by Eq. (15). Moreover, the peak shear traction can be extracted approximately from experiment as

$$\tau_0 = \frac{P_{\max}}{\pi D_f H} \tag{16}$$

where $P_{\max}$ is the peak force. It should be noted here that Eq. (16) only applies to short bonded lengths as an approximation to Eq. (14) with $c = 0$. In terms of designing the TSV specimen for the pushout experiment, perhaps the most important implication of the shear-lag analysis is that short vias are preferable for directly extracting interfacial parameters from the measured load-displacement response. Thus the bonded length of the specimen was selected to be 5 μm, with which the shear lag analysis was used to obtain a good estimate of the parameters as listed in Table II.

B. Linearly Elastic Fracture Analysis

A linearly elastic fracture analysis was conducted using the finite element package ABAQUS®in order to obtain the fracture toughness of the TSV/silicon interface and the corresponding mode-mix in the via pushout experiment. In addition, the potential for using compliance measurements as a way of measuring the crack length was explored.

The approach followed the one outlined in [16]. The model was axisymmetric (Fig. 11a) and assumed that the copper via, silicon matrix, and the diamond indenter were all linearly elastic and isotropic. The material properties used in the finite element model are listed in Table III. The initial crack length was 1μm in order to match the experimental configuration and the crack faces were modeled by contact surfaces in view of the potential for crack face contact under mode II dominant conditions [17], [18]. Eight-node quadratic elements were used for all the elements except those at the crack tip, which were singular elements. The indenter load was set at 12 mN, corresponding to the average peak value of the load measured in the experiment. The geometrical and mesh details of the finite element model are shown in Fig. 11a. The corresponding values of the stress intensity factors were obtained as: $K_{IC} = -0.56\text{GPa}\sqrt{\text{m}}$ and $K_{IIC} = 0.98\,\text{GPa}\sqrt{\text{m}}$.

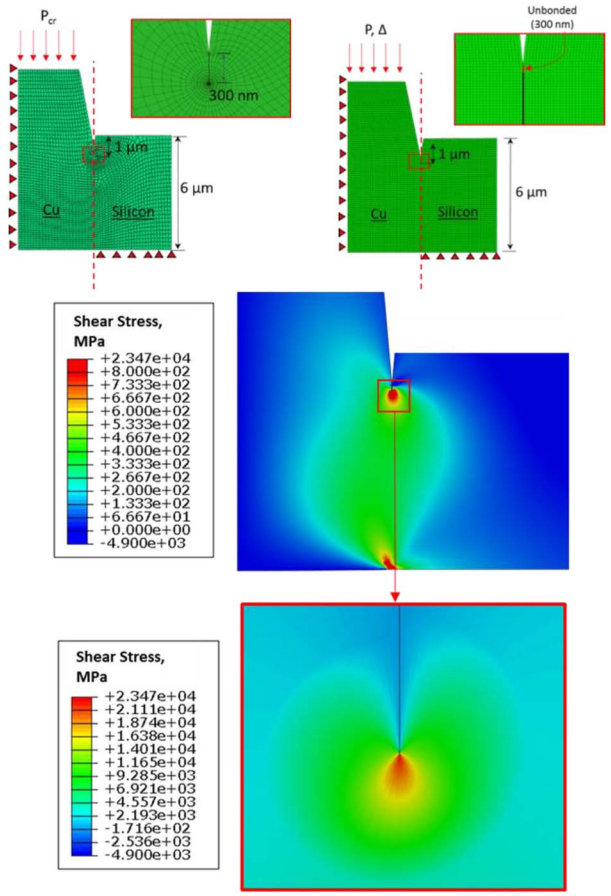

Fig. 11. Finite element model: (a) mesh for LEFM analysis; (b) mesh with cohesive elements; (c) global and local shear stress distribution from LEFM.

TABLE III
MATERIAL PROPERTIES USED IN FINITE ELEMENT ANALYSES

	Young's Modulus (GPa)	Poisson's Ratio
Cu via	110	0.28
Si	165	0.2
Diamond tip	1220	0.22

The negative value of the mode-I stress intensity factor indicates that there was indeed contact between the crack surfaces and fracture occurred under the mode II (shear) condition. The corresponding value of the J-integral (not accounting for the negative mode I stress intensity factor) was 7.9 J/m^2, which is therefore viewed as the mode II fracture toughness (J_{II}) of the TSV/silicon interface. Similar values of the fracture toughness were obtained from the shear-lag analysis as listed in Table II, by integrating the traction-separation relation up to the maximum shear traction, i.e., $J_{II} = \tau_0\delta_0/2$. From the shear stress contours (Fig. 11c), the highest shear stresses occurred at both the crack tip and the bimaterial corner between the copper and silicon at the bottom of the via. Furthermore, based on this linearly elastic analysis, the stresses exceeded the shear yield strength of the copper (216 MPa) along the entire interface which was the motivation for including the plasticity effects in the cohesive zone analysis, detailed in the Section III-C.

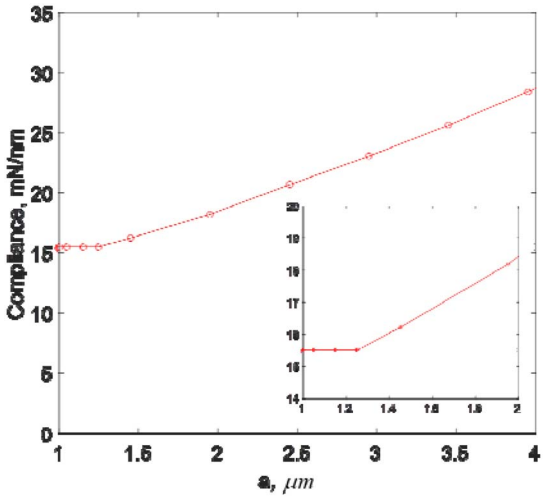

Fig. 12. The effect of crack length on specimen compliance.

The potential for using specimen compliance to track the crack length was explored by conducting finite element analyses of stationary cracks ranging from 50 nm to 4 μm for a 5 μm via. The compliance only increased by about 3% for cracks ranging from 50 nm to 1 μm (Fig. 12) but increased sharply thereafter. For displacement control, this means that the J-integral also increases with increasing crack length, which is an unstable situation. As indicated earlier, the initial crack from FIB was 1 μm and unstable growth was in fact observed in the experiments. Furthermore, the modest increase in compliance from the initial crack length made compliance measurements of crack length in the experiment unrealistic.

C. Cohesive Zone Analysis

Nonlinear finite element analysis with cohesive zone modeling provides another way to extract the interfacial properties. In doing so, it is no longer necessary to assume that the matrix is rigid. It also allows any plastic deformations in the copper to be accounted for. The finite element code ABAQUS® was again used for the analysis although the mesh was slightly modified (Fig. 11b) in order to accommodate cohesive elements ahead of the initial crack front. The silicon was still assumed to be linearly elastic and isotropic, but the stress-strain behavior of the copper followed the constitutive behavior that was extracted from the micro pillar experiment (Fig. 3). A user-defined cohesive element (UEL) subroutine was developed for the interface. Each cohesive element has four nodes, with two nodes shared with the corner nodes of a bulk silicon element and the other two with a bulk copper element. In the traction-separation relation, the separation δ is defined as the relative vectorial displacement between the nodes that are connected to the silicon and copper. In this work, it was assumed that the elastic portion of the normal and shear interactions had the same stiffness k, which ensures that the traction and displacement vectors are aligned [19]. This gives a normal traction-separation relation as $\sigma = k\delta_n$ for both tension and compression. The strength in the normal direction was assumed to be infinite. However, the shear

interaction had a finite strength $\tau_0 = k\delta_0$ corresponding to onset of sliding at a relative shear displacement δ_0. The frictional sliding shear strength was set to be τ_c when the relative shear displacement is greater than δ_0. Moreover, the via dimeter was assumed to be a constant (10 μm) over the bonded portion of the specimen but varied linearly with a 2° tapering angle for the extruded part. The possible tapering of the via in the bonded part was much smaller, and the corresponding variation in the via diameter was negligible over the short bonded length of 5 μm. Therefore, in both the analytical and numerical analysis, the effect of tapering in the bonded part of the push-out specimen was neglected.

To compare with the load-displacement responses in experiments, we set τ_c to be 25 MPa as before and slightly varied the other parameters (δ_0 and k) to best fit the response before frictional sliding. This scheme led to an average peak shear traction of 77.2 MPa for the onset of sliding. The extracted parameters are compared with those obtained using the analytical approach in Table II. It can be seen that the two sets of extracted parameters are in close agreement. It is worth noting here that the average J-integral calculated from the traction-separation relation prior to sliding is about 7.06 J/m^2, which is close to that obtained by the LEFM analysis. This shows the consistency between LEFM and cohesive zone modeling approaches on the critical J-integral. The agreement in the extracted strength values is due to the short via and the resulting unique and striking features of the force-displacement response. Both the compliance of the matrix and plasticity in the via may contribute to the stiffness of the load-displacement response. However, since τ_0 was about a third of the yield strength of the copper, the amount of plastic deformation turned out to be small. The extent of plastic deformation can be seen in the distributions of the von Misses stress and equivalent plastic strain (Fig. 13) at the peak load. It can be seen that the plastic strain was highly localized near the crack tip and therefore did not affect the global force-displacement response (Fig. 14). The numerical model also accounted for the compliance of the elastic matrix, which led to an approximately 13% increase in the stiffness of the traction-separation relation and correspondingly a smaller value for δ_0 compared to the shear lag analysis.

For the frictional sliding part, a coefficient of friction may be estimated as $\mu = \tau_c/\sigma_c$, where σ_c is the compressive normal traction at the interface and is mainly caused by the mismatch of thermal expansion between the copper via and the silicon wafer [7]. From the analytical model developed in [7], the normal traction can be estimated as

$$\sigma_c = -\Delta T(\alpha_{Cu} - \alpha_{Si})\left(\frac{1-\nu_{Cu}}{E_{Cu}} + \frac{1+\nu_{Si}}{E_{Si}}\right)^{-1} \quad (17)$$

where ΔT is the temperature change ($\sim$ 250°C) during the manufacturing process, and the coefficients of thermal expansion are: $\alpha_{Cu} = 17$ppm/°C and $\alpha_{Si} = 2.3$ ppm/°C. Note that there is another contribution to the radial traction at the interface which is due to the indentation itself. However, this was found to be more than one order of magnitude lower than the thermal contribution and hence ignored. With the extracted frictional shear strength $\tau_c = 25$ MPa, the coefficient of friction was then estimated to be 0.089.

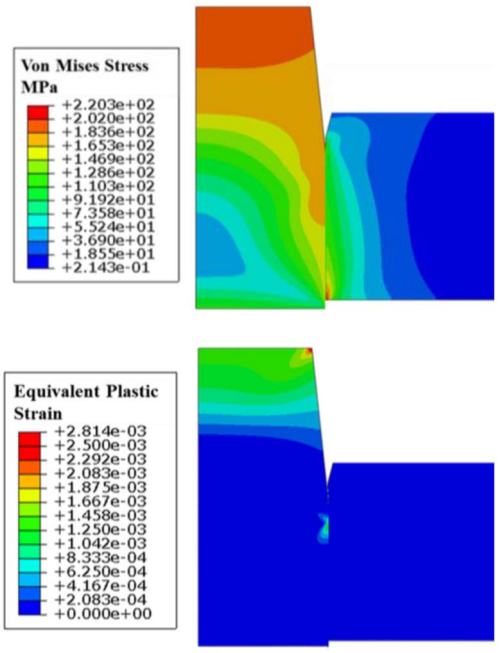

Fig. 13. Cohesive zone modeling results at the peak force: (a) Von Mises stress contour and (b) equivalent plastic strain contour.

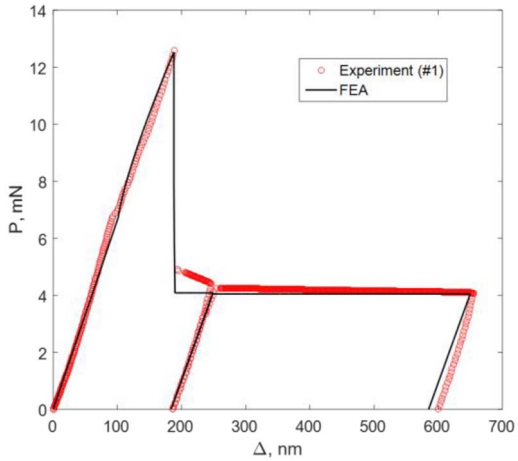

Fig. 14. Comparison of force-displacement response for Specimen #1 between cohesive zone modeling and experiment.

IV. Conclusion

This paper describes a via pushout experiment to extract the interfacial properties for shear interactions between a copper TSV and silicon. A shear lag analysis was used to develop initial estimates of the interfacial traction-separation relation including the frictional shear strength of the interface. This was followed by conducting detailed finite element analyses with cohesive zone modeling of the pushout experiment that accounted for the plasticity in the copper via and the shear interactions between copper and silicon. The average critical shear traction required to initiate interfacial sliding was found to be 77.2 MPa and the corresponding relative displacement

across the interface was 182.7 nm, while the frictional shear strength was 25 MPa. The traction-separation relation with the extracted parameters may be used to study via extrusion and associated reliability analysis for integrated TSV structures.

ACKNOWLEDGMENT

The authors are thankful to Prof. Paul S. Ho's group at the University of Texas at Austin for providing the TSV specimens.

REFERENCES

[1] P. Garrou, C. Bower, and P. Ramm, *Handbook of 3D Integration: Volumes 1 and 2—Technology and Applications of 3D Integrated Circuits*. Hoboken, NJ, USA: Wiley, 2012.

[2] T. Jiang, J. Im, R. Huang, and P. S. Ho, "Through-silicon via stress characteristics and reliability impact on 3D integrated circuits," *MRS Bull.*, vol. 40, no. 3, pp. 248–256, 2015.

[3] I. De Wolf *et al.*, "Cu pumping in TSVs: Effect of pre-CMP thermal budget," *Microelectron. Rel.*, vol. 51, nos. 9–11, pp. 1856–1859, 2011.

[4] A. Heryanto *et al.*, "Effect of copper TSV annealing on via protrusion for TSV wafer fabrication," *J. Electron. Mater.*, vol. 41, no. 9, pp. 2533–2542, 2012.

[5] J. D. Messemaeker *et al.*, "Impact of post-plating anneal and through-silicon via dimensions on Cu pumping," in *Proc. IEEE 63rd Electron. Compon. Technol. Conf.*, Las Vegas, NV, USA, 2013, pp. 586–591.

[6] T. Jiang, C. Wu, J. Im, R. Huang, and P. S. Ho, "Impact of grain structure and material properties on via extrusion in 3D interconnects," *J. Microelectron. Electron. Packag.*, vol. 12, no. 3, pp. 118–122, 2015.

[7] T. Jiang *et al.*, "Plasticity mechanism for copper extrusion in through-silicon vias for three-dimensional interconnects," *Appl. Phys. Lett.*, vol. 103, no. 21, 2013, Art. no. 211906.

[8] V. T. Bechel and N. R. Sottos, "A comparison of calculated and measured debond lengths from fiber push-out tests," *Compos. Sci. Technol.*, vol. 58, no. 11, pp. 1727–1739, 1998.

[9] H. Bei *et al.*, "Compressive strengths of molybdenum alloy micro-pillars prepared using a new technique," *Scripta Materialia*, vol. 57, no. 5, pp. 397–400, 2007.

[10] L. Alexandre *et al.*, "Optimized FIB silicon samples suitable for lattice parameters measurements by convergent beam electron diffraction," *Micron*, vol. 39, no. 3, pp. 294–301, 2008.

[11] *ABAQUS Theory Manual and Analysis User's Manual (Version 6.14)*, Dassault Systèmes Simulia Corp., Providence, RI, USA, 2014.

[12] W. Ramberg and W. R. Osgood, "Description of stress–strain curves by three parameters," Nat. Advisory Committee Aeronaut., Washington, DC, USA, Tech. Rep. 902, 1943.

[13] S. Chen *et al.*, "Protrusion of electroplated copper filled in through silicon vias during annealing process," *Microelectron. Rel.*, vol. 63, pp. 183–193, Aug. 2016.

[14] W. D. Callister and D. G. Rethwisch, *Materials Science and Engineering: An Introduction*. Hoboken, NJ, USA: Wiley, 2014.

[15] S.-K. Ryu, T. Jiang, J. Im, P. S. Ho, and R. Huang, "Thermomechanical failure analysis of through-silicon via interface using a shear-lag model with cohesive zone," *IEEE Trans. Device Mater. Rel.*, vol. 14, no. 1, pp. 318–326, Mar. 2014.

[16] C. Liang and J. W. Hutchinson, "Mechanics of the fiber pushout test," *Mech. Mater.*, vol. 14, no. 3, pp. 207–221, 1993.

[17] M. Comninou and J. Dundurs, "Effect of friction on the interface crack loaded in shear," *J. Elasticity*, vol. 10, no. 2, pp. 203–212, 1980.

[18] J. Dundurs, "Interface crack," *J. Appl. Mech. Trans. ASME*, vol. 45, no. 3, p. 700, 1978.

[19] C. Wu, S. Gowrishankar, R. Huang, and K. M. Liechti, "On determining mixed-mode traction–separation relations for interfaces," *Int. J. Fracture*, vol. 202, no. 1, pp. 1–19, 2016.

Chenglin Wu, photograph and biography not available at the time of publication.

Rui Huang, photograph and biography not available at the time of publication.

Kenneth M. Liechti, photograph and biography not available at the time of publication.